Dephasing of Strong-Field-Driven Excitonic Autler-Townes Doublets Revealed by Time- and Spectrum-Resolved Quantum-Path Interferometry

Yaxin Liu,[1,*] Bingbing Zhu,[1,*] Shicheng Jiang,[2,*,†] Shenyang Huang,[1,6] Mingyan Luo,[1] Sheng Zhang,[1] Hugen Yan,[1] Yuanbo Zhang,[1,4,5] Ruifeng Lu,[3,‡] and Zhensheng Tao[1,§]

[1]*State Key Laboratory of Surface Physics and Key Laboratory of Micro and Nano Photonic Structures (MOE), Department of Physics, Fudan University, Shanghai 200433, People's Republic of China*

[2]*State Key Laboratory of Precision Spectroscopy, East China Normal University, Shanghai 200062, People's Republic of China*

[3]*Institute of Ultrafast Optical Physics, MIIT Key Laboratory of Semiconductor Microstructure and Quantum Sensing, Department of Applied Physics, Nanjing University of Science and Technology, Nanjing 210094, People's Republic of China*

[4]*Shanghai Qi Zhi Institute, Shanghai 200232, People's Republic of China*

[5]*New Cornerstone Science Laboratory, Shenzhen 518054, People's Republic of China*

[6]*Institute of Optoelectronics, Fudan University, Shanghai 200433, People's Republic of China*

(Received 15 January 2024; revised 24 March 2024; accepted 31 May 2024; published 12 July 2024)

Understanding dephasing mechanisms of strong-field-driven excitons in condensed matter is essential for their applications in quantum-state manipulation and ultrafast optical modulations. However, experimental access to exciton dephasing under strong-field conditions is challenging. In this study, using time- and spectrum-resolved quantum-path interferometry, we investigate the dephasing mechanisms of terahertz-driven excitonic Autler-Townes doublets in MoS_2. Our results reveal a dramatic increase in the dephasing rate beyond a threshold field strength, indicating exciton dissociation as the primary dephasing mechanism. Furthermore, we demonstrate nonperturbative high-order sideband generation in a regime where the driving fields are insufficient to dissociate excitons.

DOI: 10.1103/PhysRevLett.133.026901

Introduction.—Ultrafast manipulation of electronic states in quantum materials is essential for quantum-state engineering and ultrafast optical modulation. Recently, strong-field-driven materials have exhibited fascinating tailored properties, including modification of topological states [1–6], modulation of optical properties [7–9], and band-structure engineering [10]. Among different methods, a classical approach for engineering light-matter interactions is to coherently drive a quantum three-level system with electromagnetic fields, inducing the Autler-Townes (AT) effect [11] and enabling strong and ultrafast modulation of material optical properties. In condensed matter, the AT effect has been extensively studied on excitons in GaAs quantum wells [12–15], and more recently, in transition-metal dichalcogenides which exhibit much larger binding energies [16–18].

Understanding the dephasing mechanisms of excitonic AT effects is essential for their applications in precise quantum-state manipulation and high-resolution optical spectroscopy, particularly under intense driving fields where giant optical modulations can be achieved. However, experimental methods for accessing exciton dephasing properties under strong-field excitation are lacking. Furthermore, the status of laser-dressed excitons under nonperturbative conditions also remains an unresolved question.

While phonons and many-body environments are recognized for their significant role in exciton dephasing under low-field conditions, resulting in typical dephasing times (T_2) of 0.1–1 ps and 10–100 fs, respectively [19–22], dephasing under strong-field conditions remains a subject of controversy. Recent studies on high-order harmonic generation (HHG) and sideband generation (HSG) from solids have revealed a surprisingly short T_2 of 0.1–4 fs for strong-field-dressed electrons [23–28]. The dephasing rates in these studies were often determined by comparing the decay of harmonic spectra with simulations assuming constant or $\boldsymbol{k}$-dependent dephasing rates [23,24,27]. However, this approach may be inadequate, as the contributions from electrons and holes in high-energy bands can obscure the actual dephasing dynamics of the low-energy charge carriers.

In this work, we employ the quantum-path interferometry to investigate the dephasing of an excitonic AT doublet in bulk MoS_2 driven by intense terahertz fields. The contribution of the AT doublet is distinguished by the spectrum-resolving capability of our method. The resonant transitions to the dressed excitonic states result in amplitude and phase modulations in the spectrotemporal interferograms, allowing the extraction of dephasing rates. To our knowledge, this represents the first extraction of the dephasing rates of a strong-field-driven AT doublet in condensed matter. Our findings reveal a field-strength-dependent dephasing rate for dressed excitons, with its zero-field value consistent with the relaxation pathway of

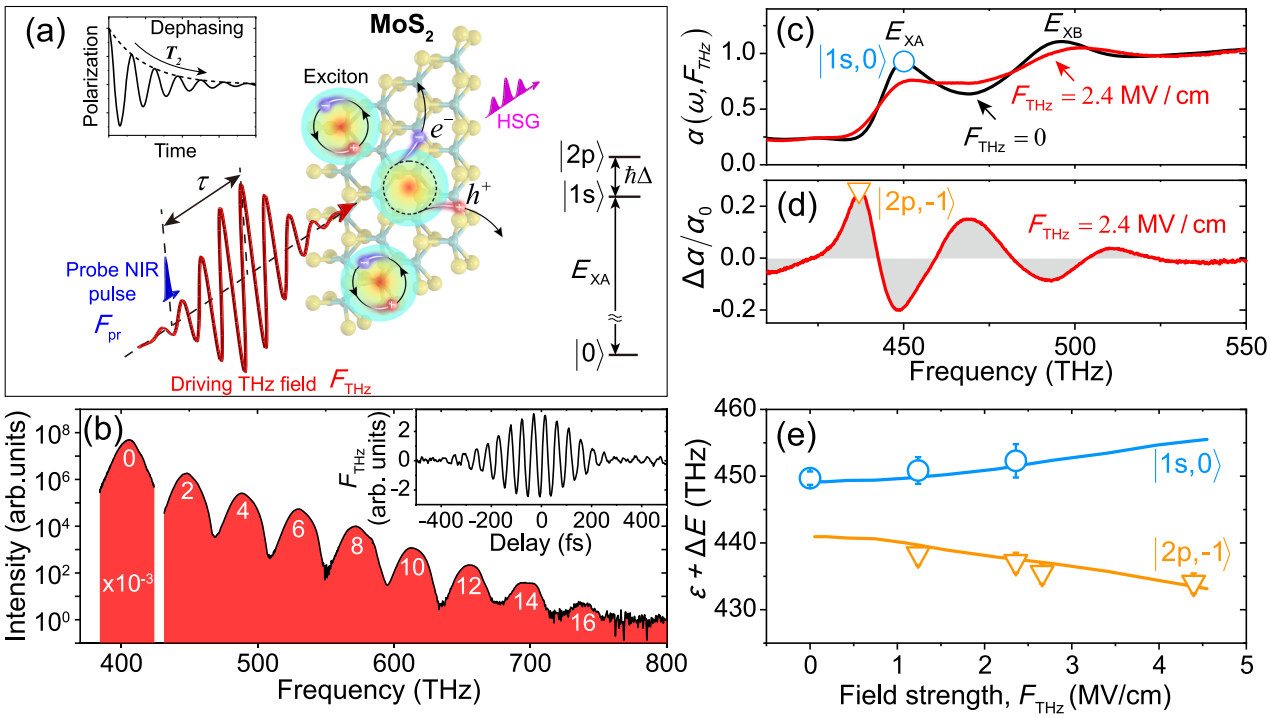

FIG. 1. (a) Experimental setup: A strong THz field is applied to drive the excitons in bulk MoS_2, and the dephasing time (T_2) is probed by HSG with a NIR probe pulse arriving at a time delay of τ. Inset: illustration of the excitonic states. (b) HSG spectrum excited by $F_{THz} = 5.0$ MV/cm. Inset: a typical electro-optic-sampling trace of the THz pulse. (c) Absorbance spectra of bulk MoS_2 with and without THz-field excitation. The absorption peak of $|1s, 0\rangle$ is labeled. (d) Normalized difference spectrum of absorbance for $F_{THz} = 2.4$ MV/cm. The absorption peak of $|2p, -1\rangle$ is labeled. (e) Summary of the $|1s, 0\rangle$ and $|2p, -1\rangle$ energies as a function of F_{THz}.

exciton-phonon interaction. Remarkably, we observe a significant increase in the dephasing rate beyond a threshold field strength of approximately 2.1 MV/cm, which allows us to identify that exciton dissociation plays a dominant role. Our results demonstrate nonperturbative HSG in a regime where the driving fields are not strong enough to dissociate the excitons.

Dressed excitonic states in bulk MoS_2.—The experiment involves exciting a 50-nm thick MoS_2 with a strong multicycle terahertz (THz) pulse (F_{THz}, red waveform) featuring a center frequency of 21 THz and a photon energy of $\hbar\Omega = 86.6$ meV [Fig. 1(a)]. The peak electric field inside the material can reach 5.6 MV/cm, with its polarization along the Γ-K direction of the Brillouin zone. A near-infrared (NIR) probe pulse (F_{pr}, blue pulse) with varying frequencies and bandwidths induces phase-locked HSG [28–30] with a photon energy of $\hbar(\omega + n\Omega)$, where ω is the probe-pulse frequency and n is the sideband order. A typical HSG spectrum under $F_{THz} = 5.0$ MV/cm is shown in Fig. 1(b), where spectral components up to the 16th order ($n = 16$) can be observed. The inset of Fig. 1(b) depicts a typical waveform of the THz driving field. Details of the experimental setup and sample preparation are summarized in the Supplemental Material [31], Sec. S1.

In Fig. 1(c), we show the absorbance, $\alpha(\omega, F_{THz})$, of MoS_2 with and without the THz-pump excitation, probing the AT doublet with a broadband NIR pulse. Under the field-free condition, the resonant feature at 448 THz (~1.85 eV) can be attributed to the transition energy of $|1s\rangle$ of the type-A exciton (E_{XA}) [43,44]. The THz field induces strong absorbance change, including the reduction and broadening of the absorption peak and a blueshift in energy (see the Supplemental Material, Sec. S3).

Because the dressing THz field oscillates at a frequency significantly lower than the bandgap, it strongly couples the $|1s\rangle$ and $|2p\rangle$ states of the Wannier-Mott excitons [inset of Fig. 1(a)]. According to the Floquet theorem [5,45], the dressed excitonic state is a superposition of equidistant energy state manifolds, containing two states, $|1s, l\rangle$ and $|2p, l-1\rangle$, in each Floquet Brillouin zone (FBZ), where l is an integer denoting the number of dressing photons (see the Supplemental Material, Fig. S7). Owing to the selection rule, $|2p, 0\rangle$ is not directly accessible, but $|2p, -1\rangle$ can be measured under the THz-field dressing. Experimentally, the absorption feature of $|2p, -1\rangle$ can be resolved by the difference spectrum $\Delta\alpha(\omega, F_{THz}) \equiv \alpha(\omega, F_{THz}) - \alpha_0(\omega)$ [Fig. 1(d)] [16,18]. In Fig. 1(e), the energy shifts ($\varepsilon + \Delta E$) of $|1s, 0\rangle$ and $|2p, -1\rangle$ under different F_{THz} are summarized, revealing clear AT-splitting features. These results can be well reproduced by simulations considering the hybridization of $|1s, l\rangle$ and $|2p, l-1\rangle$ (the solid lines), indicating resonant contributions of the dressed excitonic states in the spectral range of 430–460 THz (see the Supplemental Material, Sec. S4).

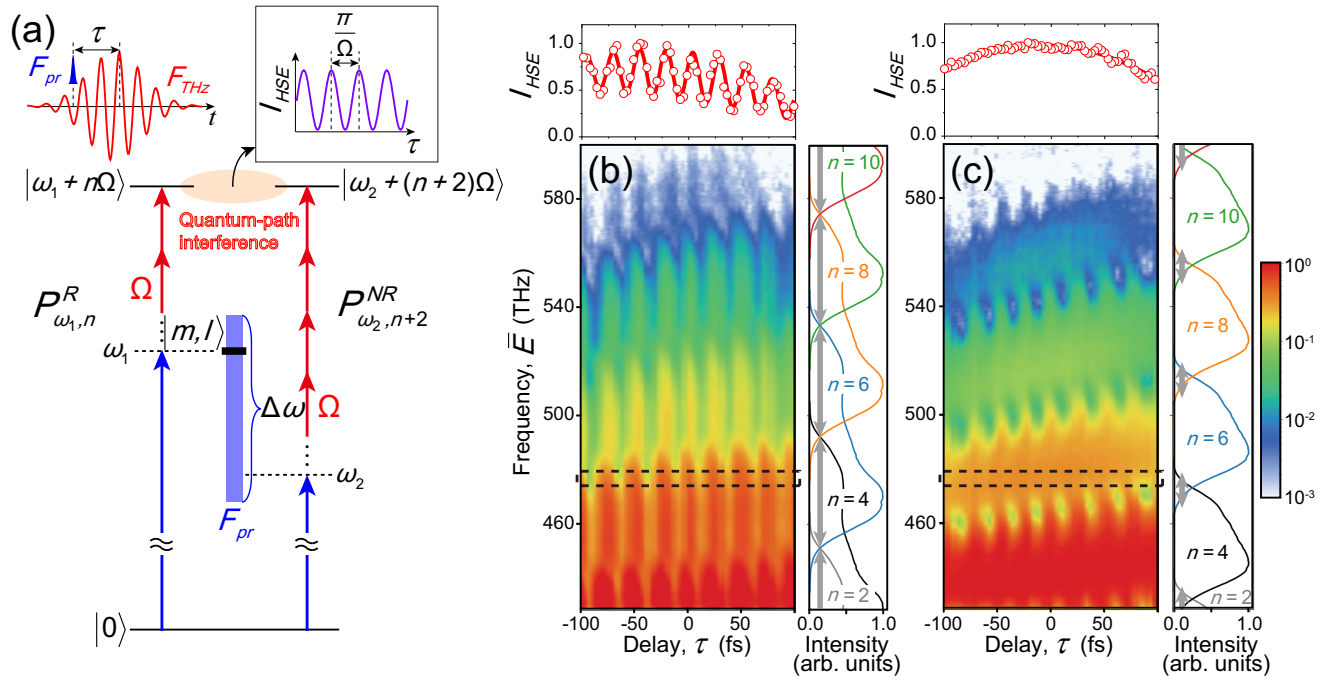

FIG. 2. (a) Illustration of QPI between HSG photon states $|\omega_1 + n\Omega\rangle$ and $|\omega_2 + (n+2)\Omega\rangle$. The quantum path of $|\omega_1 + n\Omega\rangle$ is on resonance with a dressed excitonic state $|m, l\rangle$. QPI results in the I_{HSG} oscillation as a function of τ with a period of π/Ω. (b) Spectrotemporal interferogram obtained from a 50-nm WSe_2 sample with F_{pr} bandwidth $\Delta\omega \sim 95$ THz. Right: 1D lineouts of F_{pr} spectra, upshifted by $n\Omega$ to illustrate the spectral regions for different HSG orders. Gray arrows show the quantum-path-overlapping regions. Upper: 1D lineout of I_{HSG} in the selected spectral range. (c) Similar to (b), but with a narrower bandwidth of $\Delta\omega \sim 65$ THz.

Quantum-path interferometry.—A weak NIR probe $F_{\mathrm{pr}}(\omega, \tau)$, with τ representing the time delay between the THz and probe pulses, induces polarization corresponding to the n th order sideband, denoted by $P_{\omega,n}(\omega + n\Omega, \tau) = \chi(\omega + n\Omega)F_{\mathrm{pr}}(\omega, \tau)$. Here, $\chi(\omega + n\Omega)$ is the effective susceptibility given by

$$\chi(\omega + n\Omega) = \sum_{l\in Z}^{\varepsilon_m \in \mathrm{FBZ}} \frac{V_{0m}^{l-n}(V_{0m}^{l})^*}{\varepsilon_m - \varepsilon_0 - \hbar(l\Omega + \omega) - i\Gamma_{\mathrm{ex}}^{n}}, \quad (1)$$

where V_{0m}^{l} denotes the Fourier component of the transition dipole $\langle m, l|r|0\rangle$ with $m \in \{1\mathrm{s}, 2\mathrm{p}\}$, and Γ_{ex}^{n} is a phenomenological n-dependent dephasing rate of the dressed excitons (see the Supplemental Material, Sec. S4).

As illustrated in Fig. 2(a), when the probe bandwidth $\Delta\omega$ is larger than 2Ω, two quantum paths with equal energy lead to the transitions from the vacuum state ($|0\rangle$) to two degenerate states: $|\omega_1 + n\Omega\rangle$ and $|\omega_2 + (n+2)\Omega\rangle$, where ω_1 and ω_2 fall within the bandwidth $\Delta\omega$. The interference between these paths results in the I_{HSG} oscillation as a function of τ with a period of π/Ω. The intensity oscillation can be described by

$$\begin{aligned} I_{\mathrm{HSG}}(\bar{E}, \tau) = {} & |P^{\mathrm{R}}_{\omega_1,n}(\bar{E}, \tau)|^2 + |P^{\mathrm{NR}}_{\omega_2,n+2}(\bar{E}, \tau)|^2 \\ & + 2|P^{\mathrm{R}}_{\omega_1,n}(\bar{E}, \tau)||P^{\mathrm{NR}}_{\omega_2,n+2}(\bar{E}, \tau)| \\ & \times \cos[2\Omega\tau + \Delta\phi(\bar{E}) + \Delta\varphi_{n,n+2}(\bar{E})], \end{aligned} \quad (2)$$

where $\bar{E} = \omega_1 + n\Omega = \omega_2 + (n+2)\Omega$, $P^{\mathrm{R}}_{\omega_1,n}$ and $P^{\mathrm{NR}}_{\omega_2,n+2}$ respectively denote the polarization corresponding to the resonant (R) and nonresonant (NR) transitions respectively, $\Delta\phi = \phi(\omega_1) - \phi(\omega_2)$ is the phase difference induced by F_{pr}, and $\Delta\varphi_{n,n+2} = \varphi_n - \varphi_{n+2}$ denotes the dipole phase difference. Detailed derivations are provided in the Supplemental Material, Sec. S4.

The quantum-path interferometry (QPI) scenario in Fig. 2(a) becomes evident when examining the I_{HSG} oscillations as a function of $\Delta\omega$. The experiments were conducted on a 50-nm thick WSe_2 sample to avoid exciton resonance (see below). In Fig. 2(b), with $\Delta\omega \approx 95$ THz ($>4\Omega$), fully overlapped spectra of the neighboring HSG orders exhibit 2Ω oscillation of I_{HSG} across the entire spectral range, consistent with previous work [28]. However, at reduced $\Delta\omega$ (~65 THz, with $2\Omega < \Delta\omega < 4\Omega$), both the oscillating and nonoscillating spectral regions are simultaneously observed [Fig. 2(c)]. Remarkably, the oscillating spectral regions precisely align with the regions where the quantum paths overlap (see the Supplemental Material, Sec. S6).

Our results highlight the quantum nature of transient HSG dynamics [15,46], offering a unique opportunity to access the phase of coherently driven states. In particular, when one of the interfering quantum paths resonantly couples a dressed quantum state [e.g., $P^{\mathrm{R}}_{\omega_1,n}$ in Fig. 2(a)], the resulting interferogram can provide important information about the time-domain dipole response. While a similar idea has been

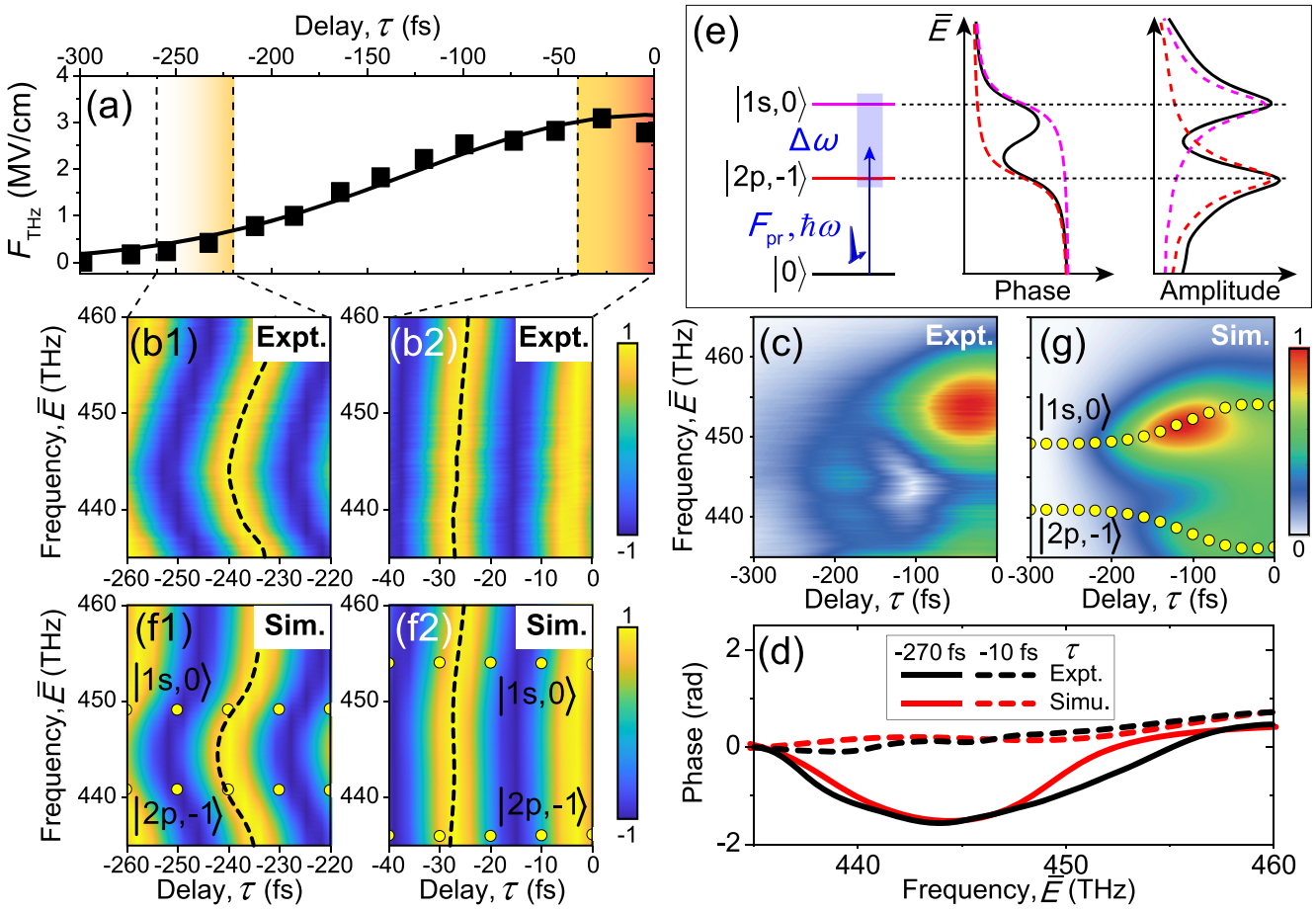

FIG. 3. (a) Envelope of the THz field. (b) Experimental 2Ω components driven by $F_{\mathrm{peak}} \approx 3$ MV/cm. (b1) 2Ω oscillation for τ between −260 and −220 fs. The dashed line highlights the phase shifts in this spectral region. (b2) Similar to (b1), for τ between −40 and 0 fs. (c) Experimental amplitudes of the 2Ω components. (d) Spectral phase of 2Ω oscillations at different τ extracted from the experimental and simulation results using the temporally resolved analysis. (e) Illustration of the phase variations and oscillation amplitudes induced by the resonant transitions to $|1\mathrm{s},0\rangle$ and $|2\mathrm{p},-1\rangle$. Dashed lines represent individual resonant transitions, and solid black lines depict the combined results. (f1),(f2) 2Ω oscillations extracted from the numerical simulations, with yellow dots labeling the shifts of $|1\mathrm{s},0\rangle$ and $|2\mathrm{p},-1\rangle$ energies. (g) Amplitudes extracted from the numerical simulations.

successfully implemented in laser-driven gas atoms [47,48] and solids [49,50], these studies have mainly focused on the high-energy region. It is noteworthy to mention that various QPI effects have attracted great attention in recent HSG studies [51–53]. Our work presents a unique opportunity to directly access the dephasing dynamics of strong-field-dressed excitons using the concept of QPI.

Dephasing of strong-field-dressed excitons.—In Fig. 3, we plot the spectrotemporal interferogram measured on the MoS_2 sample. The experimental THz-field envelope is shown in Fig. 3(a). To cover the exciton resonance, the F_{pr} spectrum spans from 330 to 465 THz. The observed 2Ω oscillation results from the overlapping $n = 0$ and 2 quantum paths (see the Supplemental Material, Sec. S7). Consequently, the I_{HSG} oscillation carries the dipole phase difference of $\Delta\varphi_{0,2}$. To illustrate the phase shifts more clearly, we remove the nonoscillating contributions by appropriate frequency filtering (see the Supplemental Material, Sec. S5). Figure 3(b1) shows the phase shifts of 2Ω oscillation for $\bar{E}$ in the range between 430 and 460 THz when τ is between −260 and −220 fs, corresponding to weak dressing fields. This energy range aligns with the resonant energies of $|1\mathrm{s},0\rangle$ and $|2\mathrm{p},-1\rangle$ at the low-field limit [Fig. 1(e)]. Notably, as τ approaches the pulse temporal center (τ between −40 and 0 fs), where F_{THz} reaches the maximum, the phase shifts in the same spectral range gradually diminish [Fig. 3(b2)]. The complete interferogram showing this evolution is provided in the Supplemental Material, Fig. S12. Correspondingly, Fig. 3c shows two peaks of the oscillation amplitudes within this spectral range.

The experimental phase variations are further supported by a temporally resolved analysis [Fig. 3(d)]. Specifically, for each sampled τ, we perform a Fourier transform in a temporal window of 25 fs and the spectral range of 435–460 THz to extract the 2Ω-component phase.

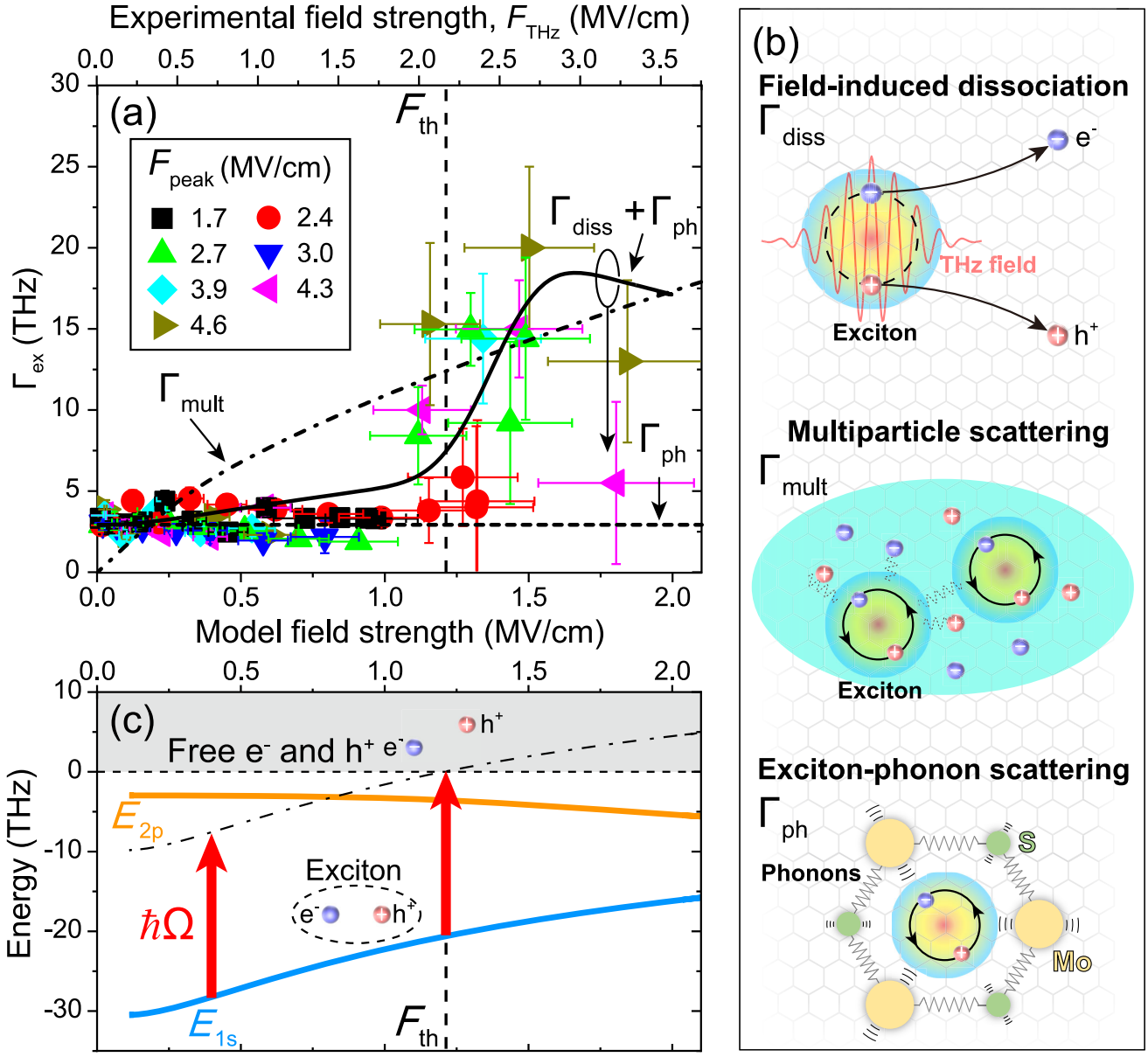

FIG. 4. (a) Summary of the dephasing rates, Γ_{ex}, under different THz-field strengths, F_{THz}. Predictions from different mechanisms are shown for comparison, with the solid line representing $\Gamma_{diss}+\Gamma_{ph}$, the dashed line for Γ_{ph}, and the dashed-dot line for Γ_{mult}. Error bars for Γ_{ex} result from the fitting errors, while those for F_{THz} stem from the experimental uncertainties. (b) Illustration of different dephasing mechanisms. (c) Model results of the eigenenergies of 1s and 2p (E_{1s} and E_{2p}) as a function of F_{THz}. Red arrows represent the transitions induced by a THz photon ($\hbar\Omega$). The dashed-dot line illustrates the upshift of E_{1s} by $\hbar\Omega$.

When $\tau=-270$ fs, we observe a robust phase shift $\Delta\varphi_{0,2}$ of -1.8 rad at $\bar{E}\approx 445$ THz, returning to 0 at $\bar{E}\approx 460$ THz. In stark contrast, the phase shift vanishes when $\tau=-10$ fs. Notably, the results at $\tau=-10$ fs demonstrate that the contribution of probe-pulse dispersion ($\Delta\phi$) is negligible here.

According to Eq. (1), the phase shifts and amplitude peaks can be attributed to the F_{pr}-induced resonant transitions from $|0\rangle$ to $|1s,0\rangle$ and $|2p,-1\rangle$ [Fig. 3(e)]. Whenever F_{pr} induces a resonant transition, a π phase shift arises, and an "S"-shape phase shift emerges when consecutive resonant transitions occur in the spectral range. Correspondingly, the spectral amplitude peaks around the resonant energies.

The diminishment of phase variations under a strong driving field can be attributed to the increased dephasing rate (Γ_{ex}). When Γ_{ex} becomes much larger than the energy separation between the two resonant states, the twisting phase shifts become no longer observable due to the dephasing-induced spectral smearing. From a different perspective, the observation of phase variations under weak driving fields here indicates that Γ_{ex} must be less than the

energy separation between $|1s, 0\rangle$ and $|2p, -1\rangle$ ($|\hbar\Omega - \hbar\Delta| \approx$ 10 THz), corresponding to $T_2 > 100$ fs.

In Fig. 4(a), we summarize the field-strength dependence of Γ_{ex}. The experimental Γ_{ex} was obtained by fitting the delay-dependent phase variations using a model that considers multiple resonant transitions (see the Supplemental Material, Sec. S4). The field strength F_{THz} was extracted at different τ of the THz transients with varying peak-field strengths, F_{peak}. The results indicate that T_2 is ~300 fs ($\Gamma_{ex} \approx 3.0$ THz), when the THz field is absent, consistent with previous low-field studies where exciton-phonon scattering is the main dephasing channel [54–56]. An intriguing observation is the significant increase in the dephasing rate when F_{THz} exceeds a threshold strength (F_{th}) of ~2.1 MV/cm. Notably, the threshold field strength has already reached the nonperturbative region (see the HSG-intensity measurement in the Supplemental Material, Sec. S2) [23,24,27,28].

To understand our results, we explore three potential exciton dephasing mechanisms [Fig. 4(b)]: multiparticle scattering (Γ_{mult}) [27], exciton-phonon scattering (Γ_{ph}) [19], and field-induced dissociation (Γ_{diss}) [57,58]. The total dephasing rate is given by $\Gamma_{ex} = \Gamma_{mult} + \Gamma_{ph} + \Gamma_{diss}$. The multiparticle and phonon environments can be theoretically evaluated using the non-Markovian semiconductor Bloch equations [59] (see the Supplemental Material, Sec. S8). The dephasing rate due to exciton dissociation is evaluated by the dissociation rate (γ_{diss}), obtained from the imaginary part of the eigenvalues in the Kramers-Henneberger frame [60] (see the Supplemental Material, Sec. S8).

Among different dephasing mechanisms, we find that only $\Gamma_{diss} + \Gamma_{ph}$ can capture the threshold behavior [Fig. 4(a)]. Our model indicates that the THz field induces an energy upshift in the stable 1s state (nonionizing), resulting in a dramatic increase in γ_{diss} when the THz photon energy ($\hbar\Omega$) aligns with the resonant transition to the continuum state [Fig. 4(c)]. In contrast, due to the accumulation effect of the THz-induced carrier density, the rise of Γ_{mult} is much slower. In our simulations [Figs. 3(d), 3(f), and 3(g)], the dephasing rate of $\Gamma_{diss} + \Gamma_{ph}$ is employed, which exhibits excellent agreement with the experimental results.

Here, our exciton-dissociation model predicts a threshold-field strength of ~1.2 MV/cm, which is lower than the experimental value [Fig. 4(a)]. This discrepancy could be attributed to the experimental uncertainties in measuring THz field strength (see the Supplemental Material, Secs. S1 and S2), as well as the dielectric screening of the material. Despite these uncertainties, our exciton-dissociation model can clearly reproduce the threshold behavior [Fig. 4(a)], which is the key to distinguish among various mechanisms.

Discussion and conclusion.—Our study employs the QPI method revealing the field-strength-dependent dephasing mechanism of excitons in bulk MoS_2, which can be attributed to the strong-field-induced exciton dissociation. Our findings demonstrate that nonperturbative HSG can occur even when the applied fields are insufficient to dissociate the excitons. Further simulations, considering field-dressed three-level excitons, indeed can reproduce HSG features, but the intensity decays dramatically beyond the second order, with band contributions dominating for higher HSG orders (see Sec. S9). Correspondingly, we no longer observe resonant amplitude or phase features associated with the AT doublet in QPI with higher HSG orders (see the Supplemental Material, Fig. S13). While previous theories have predicted HHG from bound two-level systems [61], our results indicate that signals associated with bound excitons are mainly observed in low harmonic orders, whereas higher orders are primarily contributed by band electrons.

We wish to thank Yuan Wan for valuable discussions. Z. T. acknowledges financial support from the National Key Research and Development Program of China (Grants No. 2021YFA1400200 and No. 2022YFA1404700), the National Natural Science Foundation of China (Grants No. 12221004, No. 12274091, and No. 11874121), and the Shanghai Municipal Science and Technology Basic Research Project (Grant No. 22JC1400200). R. L. acknowledges financial support from the National Key Research and Development Program of China (Grant No. 2022YFA1604301) and the National Natural Science Foundation of China (Grant No. 11974185). S. J. acknowledges the financial support from National Natural Science Foundation of China (Grant No. 12304378). Y. Z. acknowledges financial support from National Key Research and Development Program of China (Grants No. 2022YFA1403301 and No. 2018YFA0305600), Strategic Priority Research Program of Chinese Academy of Sciences (Grant No. XDB30000000), and Shanghai Municipal Science and Technology Commission (Grant No. 2019SHZDZX01). Z. T. is also thankful for the support from the Alexander-von-Humboldt Foundation.

*These authors contributed equally to this letter.
†Contact author: scjiang@lps.ecnu.edu.cn
‡Contact author: rflu@njust.edu.cn
§Contact author: ZhenshengTao@fudan.edu.cn

[1] T. Oka and H. Aoki, Phys. Rev. B **79**, 081406(R) (2009).
[2] N. H. Lindner, G. Refael, and V. Galitski, Nat. Phys. **7**, 490 (2011).
[3] J. W. McIver, B. Schulte, F. U. Stein, T. Matsuyama, G. Jotzu, G. Meier, and A. Cavalleri, Nat. Phys. **16**, 38 (2020).
[4] M. Claassen, D. M. Kennes, M. Zingl, M. A. Sentef, and A. Rubio, Nat. Phys. **15**, 766 (2019).
[5] M. S. Rudner and N. H. Lindner, Nat. Rev. Phys. **2**, 229 (2020).
[6] Y. H. Wang, H. Steinberg, P. Jarillo-Herrero, and N. Gedik, Science **342**, 453 (2013).

[7] E. J. Sie, J. W. McLver, Y. H. Lee, L. Fu, J. Kong, and N. Gedik, Nat. Mater. **14**, 290 (2015).
[8] J. Kim, X. Hong, C. Jin, S. F. Shi, C. Y. S. Chang, M. H. Chiu, L. J. Li, and F. Wang, Science **346**, 1205 (2014).
[9] J. Y. Shan, M. Ye, H. Chu, S. Lee, J. G. Park, L. Balents, and D. Hsieh, Nature (London) **600**, 235 (2021).
[10] S. Zhou, C. Bao, B. Fan, H. Zhou, Q. Gao, H. Zhong, T. Lin, H. Liu, P. Yu, P. Tang, S. Meng, W. Duan, and S. Zhou, Nature (London) **614**, 75 (2023).
[11] S. H. Autlert and C. H. Townes, Phys. Rev. **100**, 703 (1955).
[12] A. Liu and C.-Z. Ning, J. Opt. Soc. Am. B **17**, 433 (2000).
[13] S. G. Carter, V. Birkedal, C. S. Wang, L. A. Coldren, A. V. Maslov, D. S. Citrin, and M. S. Sherwin, Science **310**, 651 (2005).
[14] M. Wagner, H. Schneider, D. Stehr, S. Winnerl, A. M. Andrews, S. Schartner, G. Strasser, and M. Helm, Phys. Rev. Lett. **105**, 167401 (2010).
[15] K. Uchida, T. Otobe, T. Mochizuki, C. Kim, M. Yoshita, H. Akiyama, L. N. Pfeiffer, K. W. West, K. Tanaka, and H. Hirori, Phys. Rev. Lett. **117**, 277402 (2016).
[16] Y. Kobayashi, C. Heide, A. C. Johnson, V. Tiwari, F. Liu, D. A. Reis, T. F. Heinz, and S. Ghimire, Nat. Phys. **19**, 171 (2023).
[17] P. D. Cunningham, A. T. Hanbicki, T. L. Reinecke, K. M. McCreary, and B. T. Jonker, Nat. Commun. **10**, 5539 (2019).
[18] C. K. Yong, M. I. B. Utama, C. S. Ong, T. Cao, E. C. Regan, J. Horng, Y. Shen, H. Cai, K. Watanabe, T. Taniguchi, S. Tongay, H. Deng, A. Zettl, S. G. Louie, and F. Wang, Nat. Mater. **18**, 1065 (2019).
[19] Z. Nie, R. Long, L. Sun, C. Huang, J. Zhang, and Q. Xiong, ACS Nano **8**, 10931 (2014).
[20] S. Aeschlimann, S. A. Sato, R. Krause, M. Chávez-Cervantes, U. De Giovannini, H. Hübener, S. Forti, C. Coletti, K. Hanff, K. Rossnagel, A. Rubio, and I. Gierz, Nano Lett. **21**, 5028 (2021).
[21] H. Dehghani, T. Oka, and A. Mitra, Phys. Rev. B **90**, 195429 (2014).
[22] I. Gierz, F. Calegari, S. Aeschlimann, M. Chávez Cervantes, C. Cacho, R. T. Chapman, E. Springate, S. Link, U. Starke, C. R. Ast, and A. Cavalleri, Phys. Rev. Lett. **115**, 086803 (2015).
[23] G. Vampa and T. Brabec, J. Phys. B At. Mol. Opt. Phys. **50**, 083001 (2017).
[24] G. Vampa, C. R. McDonald, G. Orlando, D. D. Klug, P. B. Corkum, and T. Brabec, Phys. Rev. Lett. **113**, 073901 (2014).
[25] T. T. Luu, M. Garg, S. Yu. Kruchinin, A. Moulet, M. T. Hassan, and E. Goulielmakis, Nature (London) **521**, 498 (2015).
[26] M. Hohenleutner, F. Langer, O. Schubert, M. Knorr, U. Huttner, S. W. Koch, M. Kira, and R. Huber, Nature (London) **523**, 572 (2015).
[27] C. Heide, Y. Kobayashi, A. C. Johnson, F. Liu, T. F. Heinz, D. A. Reis, and S. Ghimire, Optica **9**, 512 (2022).
[28] F. Langer, M. Hohenleutner, C. P. Schmid, C. Poellmann, P. Nagler, T. Korn, C. Schüller, M. S. Sherwin, U. Huttner, J. T. Steiner, S. W. Koch, M. Kira, and R. Huber, Nature (London) **533**, 225 (2016).
[29] B. Zaks, R. B. Liu, and M. S. Sherwin, Nature (London) **483**, 580 (2012).
[30] R.-B. Liu and B.-F. Zhu, AIP Conf. Proc. **893**, 1455 (2007).
[31] See Supplemental Material at http://link.aps.org/supplemental/10.1103/PhysRevLett.133.026901 for a detailed description of the experimental and theoretical methods, which includes Refs. [32–42].
[32] M. Knorr, J. Raab, M. Tauer, P. Merkl, D. Peller, E. Wittmann, E. Riedle, C. Lange, and R. Huber, Opt. Lett. **42**, 4367 (2017).
[33] A. Ayari, E. Cobas, O. Ogundadegbe, and M. S. Fuhrer, J. Appl. Phys. **101**, 014507 (2007).
[34] H. Li, J. Wu, X. Huang, G. Lu, J. Yang, X. Lu, Q. Xiong, and H. Zhang, ACS Nano **7**, 10344 (2013).
[35] S. Roddaro, P. Pingue, V. Piazza, V. Pellegrini, and F. Beltram, Nano Lett. **7**, 2707 (2007).
[36] D. B. S. Soh, C. Rogers, D. J. Gray, E. Chatterjee, and H. Mabuchi, Phys. Rev. B **97**, 165111 (2018).
[37] G. Engelhardt and J. Cao, Phys. Rev. Lett. **126**, 090601 (2021).
[38] L. D. A. Landau and E. M. Lif, *Quantum Mechanics Non-Relativistic Theory*, 3rd ed., Course of Theoretical Physics Vol. 3 (Butterworth-Heinemann, Oxford, 1981).
[39] M. Marinescu and M. Gavrila, Phys. Rev. A **53**, 2513 (1996).
[40] M. Gavrila, *Atoms in Intense Laser Fields* (New York, 1992).
[41] N. Saigal and S. Ghosh, Appl. Phys. Lett. **106**, 182103 (2015).
[42] H. P. Komsa and A. V. Krasheninnikov, Phys. Rev. B **86**, 241201(R) (2012).
[43] E. Fortin and F. Raga, Phys. Rev. B **11**, 905 (1975).
[44] V. Jindal, D. Jana, T. Deilmann, and S. Ghosh, Phys. Rev. B **102**, 235204 (2020).
[45] J. H. Shirley, Phys. Rev. **138**, B979 (1965).
[46] N. Yoshikawa, K. Nagai, K. Uchida, Y. Takaguchi, S. Sasaki, Y. Miyata, and K. Tanaka, Nat. Commun. **10**, 3709 (2019).
[47] K. Klünder, J. M. Dahlström, M. Gisselbrecht, T. Fordell, M. Swoboda, D. Guénot, P. Johnsson, J. Caillat, J. Mauritsson, A. Maquet, R. Taïeb, and A. L'Huillier, Phys. Rev. Lett. **106**, 143002 (2011).
[48] V. Gruson, L. Barreau, Jiménez-Galan, F. Risoud, J. Caillat, A. Maquet, B. Carré, F. Lepetit, J. F. Hergott, T. Ruchon, L. Argenti, R. Taïeb, F. Martín, and P. Salières, Science **354**, 734 (2016).
[49] Z. Tao, C. Chen, T. Szilvási, M. Keller, M. Mavrikakis, H. Kapteyn, and M. Murnane, Science **353**, 62 (2016).
[50] R. Locher, L. Castiglioni, M. Lucchini, M. Greif, L. Gallmann, J. Osterwalder, M. Hengsberger, and U. Keller, Optica **2**, 405 (2015).
[51] Q. Wu and M. S. Sherwin, Phys. Rev. B **107**, 174308 (2023).
[52] S. D. O'Hara, J. B. Costello, Q. Wu, K. West, L. Pfeiffer, and M. S. Sherwin, Phys. Rev. B **109**, 054308 (2024).
[53] J. B. Costello, S. D. O'Hara, Q. Wu, M. Jang, L. N. Pfeiffer, K. W. West, and M. S. Sherwin, Phys. Rev. B **108**, 195205 (2023).
[54] G. Moody, C. Kavir Dass, K. Hao, C. H. Chen, L. J. Li, A. Singh, K. Tran, G. Clark, X. Xu, G. Berghäuser, E. Malic, A. Knorr, and X. Li, Nat. Commun. **6**, 8315 (2015).

[55] T. Jakubczyk, G. Nayak, L. Scarpelli, W. L. Liu, S. Dubey, N. Bendiab, L. Marty, T. Taniguchi, K. Watanabe, F. Masia, G. Nogues, J. Coraux, W. Langbein, J. Renard, V. Bouchiat, and J. Kasprzak, ACS Nano **13**, 3500 (2019).
[56] K. J. Czech, B. J. Thompson, S. Kain, Q. Ding, M. J. Shearer, R. J. Hamers, S. Jin, and J. C. Wright, ACS Nano **9**, 12146 (2015).
[57] H. C. Kamban and T. G. Pedersen, Phys. Rev. B **100**, 045307 (2019).
[58] M. Massicotte, F. Vialla, P. Schmidt, M. B. Lundeberg, S. Latini, S. Haastrup, M. Danovich, D. Davydovskaya, K. Watanabe, T. Taniguchi, V. I. Fal'ko, K. S. Thygesen, T. G. Pedersen, and F. H. L. Koppens, Nat. Commun. **9**, 1633 (2018).
[59] S. Y. Kruchinin, Phys. Rev. A **100**, 043839 (2019).
[60] M. Gavrila and J. Z. Kamiński, Phys. Rev. Lett. **52**, 613 (1984).
[61] B. Sundaram and P. W. Milonni, Phys. Rev. A **41**, 6571 (1990).